Journal of Applied Polymer Science

# Novel poly(vinylidene fluoride)/thermoplastic polyester elastomer composite membrane prepared by the electrospinning of nanofibers onto a dense membrane substrate for protective textiles

**Fanglong Zhu, Qun Xin, Qianqian Feng, Yu Zhou, Rangtong Liu**
College of Textile and Clothing, Zhongyuan University of Technology, Zhengzhou 450007, China
Correspondence to: F. Zhu (E-mail: 18003868331@163.com)

**ABSTRACT:** Conventionally, electrospun thin-film composite (TFC) membranes used in protective clothing are fabricated on the basis of an electrospinning substrate coated with a nonporous hydrophilic polymer layer. However, the incompatibility of common coating solvents with inertia substrate materials requires that the support material should be surface-modified to promote the crosslinking of the dense and porous layers. In this study, we attempted to fabricate a novel TFC membrane for use in protective clothing by the one-step deposition of poly(vinylidene fluoride) (PVDF) nanofibers onto a dense, hydrophilic thermoplastic polyester elastomer (TPEE) membrane substrate via electrospinning. The proposed approach has the advantage of no need for further surface modification of the substrate membrane. The optimized TFC membrane exhibited a better tensile strength than the dense substrate TPEE film. The testing results for the moisture resistance show that the new TFC membrane had a comparatively high water vapor transmission rate, notwithstanding that the value was slightly lower than that of the single-layered TPEE film. Simultaneously, a resistance-in-series model based on Henis–Tripodi's model for explaining the water vapor permeation behavior of the TFC membrane was proposed. The moisture resistance values predicted by the analyzed model were in good agreement with these experimental data. This verified the validity of this in-series moisture resistance model for the TFC membrane. The influence of the PVDF porosity on the water vapor permeation resistance throughout the TFC membrane was calculated and is discussed. More work is needed to establish the applicability of the new TFC membrane for lamination with nonwoven fabric to form the multilayered fabrics used in firefighters' protective clothing. © 2015 Wiley Periodicals, Inc. J. Appl. Polym. Sci. **2015**, *132*, 42170.

**KEYWORDS:** electrospinning; films; membranes; porous materials

Received 15 November 2014; accepted 2 March 2015
**DOI: 10.1002/app.42170**

## INTRODUCTION

Traditionally, thin-film composite (TFC) membranes have been investigated for use in water reuse and desalination processes, such as reverse osmosis[1,2] and the ultrafiltration field.[3,4] Recently, the special design of TFC membranes has emerged as a potential method for creating protective textiles embedded with breathable film; this can restrict the permeation of aerosols, liquids, and toxic gas but allow the water vapor to escape.[5] TFC-membrane-based protective fabrics are typically made up of a dense, nonporous layer coated on top of a porous layer on top of a nonwoven fabric support sheet, as is shown in Figure 1. The three-layered configuration gives the desired properties of the high rejection of undesired materials (hazardous chemicals), high filtration efficiency, and good mechanical strength. The bottom porous layer is responsible for resistance to liquid penetration and the allowance of water molecular diffusion through the polymer matrix, with the difference in the water vapor concentration across the film as the driving force.[6] The nanopores or micropores of the porous membrane provide good moisture- and vapor-release properties. However, the micropores within the porous membrane are easily jammed by contaminations and chemicals when protective clothing materials are exposed to variety of biological and chemical hazards. This prevents water vapor diffusion through the layered fabrics and results in a poor water vapor transmission (WVT) rate. A caulking layer can be applied to the porous membrane to alleviate the effects of the structural defects. That is, the addition of a hydrophilic, selective layer to the porous layer forming the TFC membrane can solve the fouling problem.

At present, two kinds of methods are commonly used to prepare the TFC membranes used in protective clothing: the costretching technique and the coating approach. These techniques were proposed by Hao *et al.*;[5,7] they coated a polyurethane (PU) film onto a PTFE membrane and costretched the composite

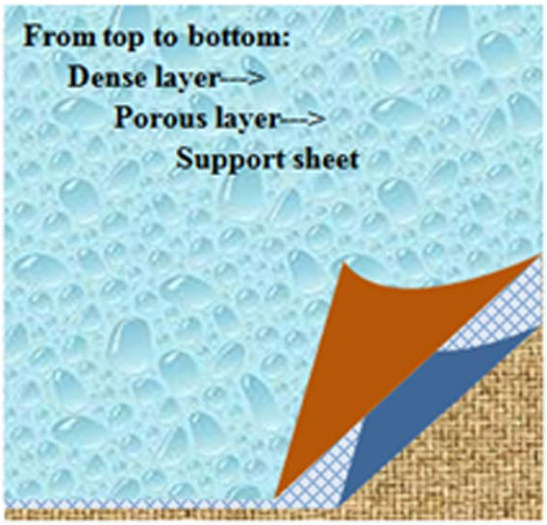


**Figure 1.** Schematic diagram of the TFC membrane-based protective fabric. [Color figure can be viewed in the online issue, which is available at wileyonlinelibrary.com.]

materials to produce protective clothing materials. However, the TFC membranes prepared by these two methods suffered from disadvantages, such as incompatibility and low adhesion strength. In other chemical industries, such as filtration applications, some researchers have attempted to apply dense polymer materials as coating materials. Yu *et al.*[8] used the plasma polymerization of ethylenediamine on a PTFE film surface to incorporate amino groups onto the PTFE surfaces. The presence of amino groups on the PTFE substrates provided chemical linkages between the PTFE and polyamide layers in interfacial polymerization to form the TFC membrane. Jiang *et al.*[9] reported the use of a PU–poly(vinylidene fluoride) (PVDF) TFC membrane for gas separation by taking the advantage of highly selective PU with its compatible PVDF.

Compared with the traditional method, the electrospinning technique has attracted much attention as a viable process for creating submicroscale to nanoscale fibers through the application of a high voltage to a polymer solution/melt. The approach provides an ultrathin, membranelike web of extremely fine fibers with a very small pore size; this is attractive for a variety of applications, from textiles to biomaterials, ultrafiltration, and reinforced composites.[10–14] Research results have indicated that the ultrathin membranelike web possessed excellent barrier performance against toxins in aerosol form and simultaneously maintained a high WVT rate. However, these pores within the electrospinning nanofibrous membranes are prone to jamming when exposed to contaminations.[15] An existing approach for solving the fouling problem is the utilization of a hydrophilic coating to change the nanofibrous membrane surface. Yoon *et al.*[4] demonstrated a new type of high-flux ultrafiltration membrane on the basis of electrospinning nanofibrous polyacrylonitrile scaffolds coupled with a thin top layer of a hydrophilic, water-resistant but water-permeable coating. Bui *et al.*[16] successfully polymerized a polyamide film over an electrospinning nanofiber nonwoven supporting; it provided superior water flux and low salt flux for engineered osmosis applications.

In this study, we proposed a new approach and first attempted to deposit a PVDF solution onto a commercial thermoplastic polyester elastomer (TPEE) film, which was used as the substrate on the basis of electrospinning technology instead of coating. TPEE consists of alternating hard polyester segments and soft flexible soft segments; this means it offers a wide range of variability in its structure and properties. In particular, TPEE with poly(ethylene oxide) soft segments is intended for use in breathable membranes, and it provides an impermeable waterproof layer for fabric laminations. Breathable TPEE films offer the advantage of a continuous, monolithic structure; this permits moisture and water vapor to evaporate and prevents liquids and even microscopic particles from permeating the lamination. Various polymers, including polysulfone and poly(-ether sulfone), have been widely used as membrane materials. PVDF has also received a great deal of attention because of its excellent chemical resistance, good thermal stability, superhydrophobicity [high contact angle (CA)], well-controlled porosity, and outstanding mechanical properties.[17] So far, PVDF has been commonly used in membrane distillation and polymer electrolytes,[18,19] but PVDF electrospun nanofibrous membranes have seldom been used as separating layers in textiles. Therefore, PVDF was selected as the material for the electrospinning membranes used in protective fabrics in this study.

In the last section in this article, we establish a moisture diffusion resistance model for a selectively permeable TFC membrane based on Henis–Tripodi's model to investigate the effects of structural parameters on the water vapor permeation throughout the TFC membrane. Simultaneously, the experimental values were also compared with the theoretically predicted results. Then, the relationship between the PVDF porosity and the water vapor permeation properties of the thin film was discussed on the basis of the proposed model.

## EXPERIMENTAL

### Materials

The membrane materials, a commercial polymer PVDF with a weight-average molecular weight of about 339,000 g/mol, were purchased from Solvay. *N,N*-Dimethylacetamide (DMAc) was purchased from Guangdong Guang Hua Technology Co., Ltd., and acetone purchased from Tianjin Fuyu Fine Chemical Co., Ltd., was used as the solvent for PVDF nanofiber electrospinning. The polyacrylate rubber used for the crosslinker was purchased from Suining Qinglong Polyacrylate Rubber Manufactory. The commercial nonporous, dense TPEE membranes (Easytex, FSPG Hi-Tech Co., Ltd., China) were used as the substrate material for the TFC membranes. TPEE is composed of poly(butylene terephthalate) (PBT) as the hard segment and polyether or polyester as the soft segment. The typical structure of TPEE is illustrated in Figure 2.[20] The TPEE membrane exhibited high water vapor permeability because of the hydrophilic group in the soft segment.

### TFC Membrane Preparation

A PVDF nanoporous membrane was deposited on a nonporous, hydrophilic substrate membrane at room temperature, as follows. PVDF was dissolved in dimethylformamide to a certain concentration. The weighted crosslinking agent (ACM) was

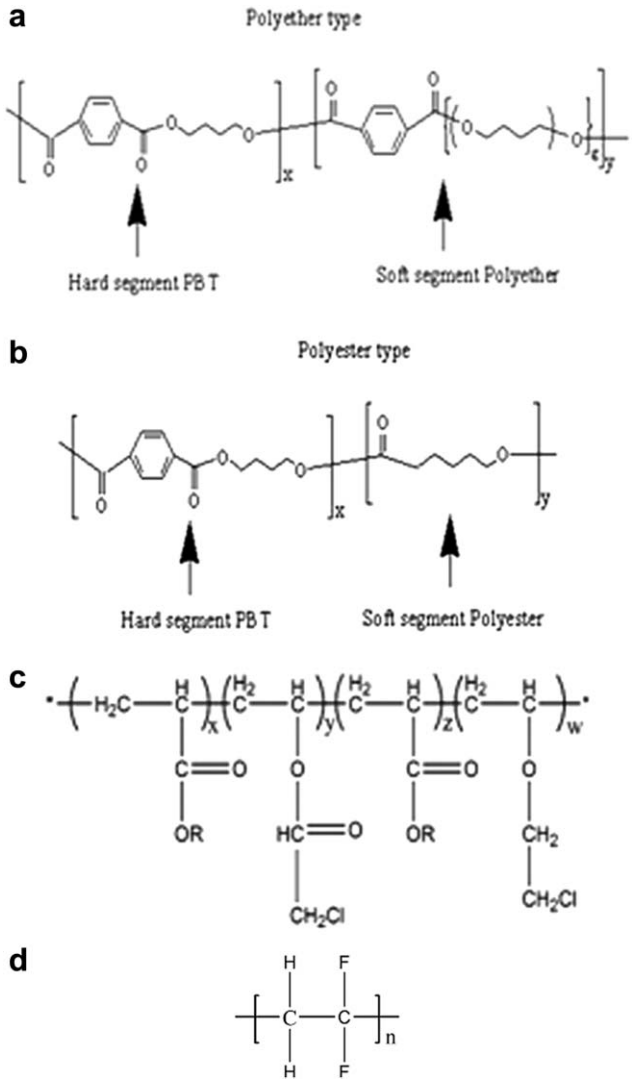


**Figure 2.** Chemical structures of the (a) TPEE copolymer, (b) block copolymer, (c) ACM, and (d) PVDF.

added to the PVDF solution. This PVDF solution was then stirred continuously for 2 h before electrospinning (Figure 3). A syringe pump (JZB-1800, JianYuan Scientific, China) was used to supply a constant flow of 1 mL/h polymer solution during electrospinning. The needle had an inner diameter of 0.41 mm. Different voltages (BGG, Beijing Supervoltage Technique, Inc., China) were applied to draw the nanofibers from the prepared solution according to the orthogonal experimental design.

### Orthogonal Experimental Design

A series of experiments on PVDF/ACM solutions with different concentrations/compositions were conducted to determine the optimum electrospinning conditions for fabrication of the thin PVDF nanofiber film. With the use of orthogonal arrays to design an experimental matrix, it is possible to vary a large number of parameters simultaneously in a designed experiment with a relatively small number of experimenta1 runs and be able to separately estimate the effects of each of the parameters on a response variable.[21] Here, an orthogonal experimental design method was applied to discuss the mass concentration of

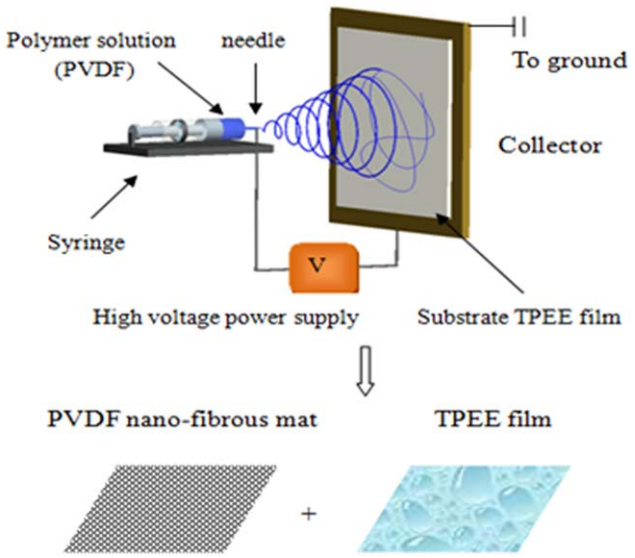


**Figure 3.** Schematic diagram of an electrospinning setup. [Color figure can be viewed in the online issue, which is available at wileyonlinelibrary.com.]

PVDF and the impact degree of the electrospinning parameters on the nanofiber structure. The mass concentration of PVDF, the electrostatic field voltage, the ratio of DMAc to acetone, the quantity of ACM, and the receiving distance were determined as the five factors of the orthogonal experiment, and each factor had four levels, as shown in Table I. The orthogonal array for the 16 PVDF membranes is tabulated in Table II; it was designed according to the orthogonal design table $L_{16}$ ($4^5$).

To swell the bonding intensity between the nanofibrous membrane and the dense membrane, the TFC membrane was then thermally pressed with an electric iron at a high temperature of 130°C for less than 10 s to incur the crosslinking reaction. The corresponding nanofibrous membranes were labeled 1 and 2 to 11 and 12, respectively.

### General Characterizations of the TFC Membrane

**Scanning Electron Microscopy (SEM).** A scanning electron microscope (JSM-6390LV, Japan) was used to investigate the morphology of the TFC membrane, and Smile View software was used for imaging. Before imaging, the samples were frozen in liquid nitrogen and sputter-coated with a layer of gold to increase their conductivity for SEM observation. The average diameters of the nanofibers were examined from more than 50

**Table I.** Factors and Levels of the 16 PVDF Nanofibrous Mats

| | Factor | | | | |
|---|---|---|---|---|---|
| Level *i* | *A* | *B* | *C* | *D* | *E* |
| 1 | 11 | 6 | 1:1 | 0.2 | 12 |
| 2 | 13 | 8 | 3:2 | 0.3 | 14 |
| 3 | 15 | 10 | 7:3 | 0.4 | 16 |
| 4 | 17 | 12 | 4:1 | 0.5 | 18 |

*A*, *B*, *C*, *D*, and *E* represent the mass concentration of PVDF, electrostatic field voltage, ratio of DMAc to acetone, quantity of ACM, and receiving distance, respectively.

**Table II.** $L_{16}$ ($4^5$) Orthogonal Array and Experimental Results

| Experiment | A | B | C | D | E | Fiber diameter (nm) |
|---|---|---|---|---|---|---|
| 1 | 1 | 1 | 1 | 1 | 1 | 0 |
| 2 | 1 | 2 | 2 | 2 | 2 | 2525 |
| 3 | 1 | 3 | 3 | 3 | 3 | 0 |
| 4 | 1 | 4 | 4 | 4 | 4 | 0 |
| 5 | 2 | 1 | 2 | 3 | 4 | 4350 |
| 6 | 2 | 2 | 1 | 4 | 3 | 1800 |
| 7 | 2 | 3 | 4 | 1 | 2 | 2050 |
| 8 | 2 | 4 | 3 | 2 | 1 | 2800 |
| 9 | 3 | 1 | 3 | 4 | 2 | 1250 |
| 10 | 3 | 2 | 4 | 3 | 1 | 4917 |
| 11 | 3 | 3 | 1 | 2 | 4 | 2875 |
| 12 | 3 | 4 | 2 | 1 | 3 | 2000 |
| 13 | 4 | 1 | 4 | 2 | 3 | 2875 |
| 14 | 4 | 2 | 3 | 1 | 4 | 1500 |
| 15 | 4 | 3 | 2 | 4 | 1 | 3375 |
| 16 | 4 | 4 | 1 | 3 | 2 | 3100 |

*A, B, C, D,* and *E* represent the mass concentration of PVDF, electrostatic field voltage, ratio of DMAc to acetone, quantity of ACM, and receiving distance, respectively.

measurements for the nanofibers at different spots on the membrane.

**CA.** The hydrophobicity or hydrophilicity of the membrane sample was determined with a video-supported CA measuring instrument (OCA20, Dataphysics, Germany) at ambient temperature. The water droplet (2.0 $\mu$L) was dropped carefully on the surface of membrane with a microsyringe, and at least six measurements were performed at different spots of the fiber mats. A magnified image of the droplet was recorded by a digital camera. The samples were dried in air before the CA tests.

**Membrane Porosity.** To measure the membrane porosity, the polymer was dissolved in pure impregnant to prepare nonporous membrane. First, the density of the nonporous membrane was determined on the basis of a weighted method and was recognized as the density of the bulk polymer. Then, the density of the composite membrane was estimated from an average of four samples. Then, the porosity of each sample was calculated with the following equation:

$$\varepsilon=(1-\frac{\rho_m}{\rho_p})\times 100\% \quad (1)$$

where $\rho_m$ is the apparent density of the membrane and $\rho_p$ is the density of the polymer.

**Membrane Mechanical Strength.** The mechanical properties of the TPEE membrane and composite membrane were examined at a temperature 20 ± 2°C in an Instron (model 5582) universal tensile tester. The effective tensile length was 25 mm, and the crosshead speed was 5 mm/min. The samples were tensile-shaped doubled blades with a size of 50 × 10 $mm^2$. The applied load and elongation were recorded.

**Attenuated Total Reflectance (ATR)–Fourier Transform Infrared (FTIR) Characterization.** ATR--FTIR analysis on the substrate film and TFC membrane surfaces were performed with a Thermo Nicolet X700 FTIR instrument with 16 repeated tests. For the ACM and PVDF raw materials, spectra were taken in the form of solution spreading over potassium bromide.

**WVT Tests.** In this study, a series of experiments were carried out to investigate the intrinsic moisture resistance ($R_m$) of the membrane samples with a covered upright dish method based on the ASTM E 96 standard approach.[22] In this method, we used a cup containing distilled water and covered it with the testing sample. The cup with sample was then put into a controlled environment chamber (Figure 4). First, the whole assembly was weighed before the test. After 24 h, the whole assembly was then reweighed. WVT ($g/m^2/day$) could be expressed by the weight change of water in the cup. The total moisture resistance ($R_t$) of the membrane sample could be written as follows:

$$R_t=18723/WVT. \quad (2)$$

All of these tests were conducted under a nonisothermal environment with an air temperature of 23°C, a RH of 50%, and a wind speed of 2.80 m/s. The temperature of water in the cup was kept at a constant value of 32°C as maintained in a constant-temperature bath. Moisture diffused through the membrane because of the vapor concentration difference between the two sides of the sample. $R_t$ could be represented by the convective moisture transfer resistance over the membrane ($R_{up}$), $R_m$ through the specimen, and the moisture resistance caused by the air gap between the water surface and sample inner surface ($R_{in}$):

$$R_t=R_{up}+R_m+R_{in}. \quad (3)$$

From eq. (3), we could calculate $R_m$ of the sample by subtracting the two moisture resistances of $R_{up}$ and $R_{in}$ from $R_t$:

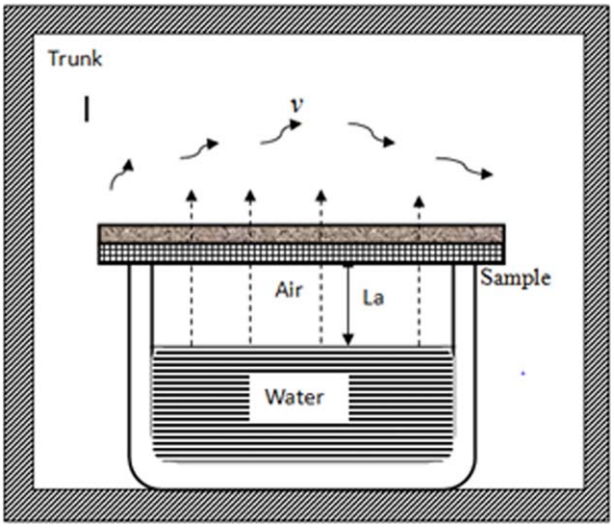


**Figure 4.** Schematic of the water vapor permeation experimental setup. [Color figure can be viewed in the online issue, which is available at wileyonlinelibrary.com.]

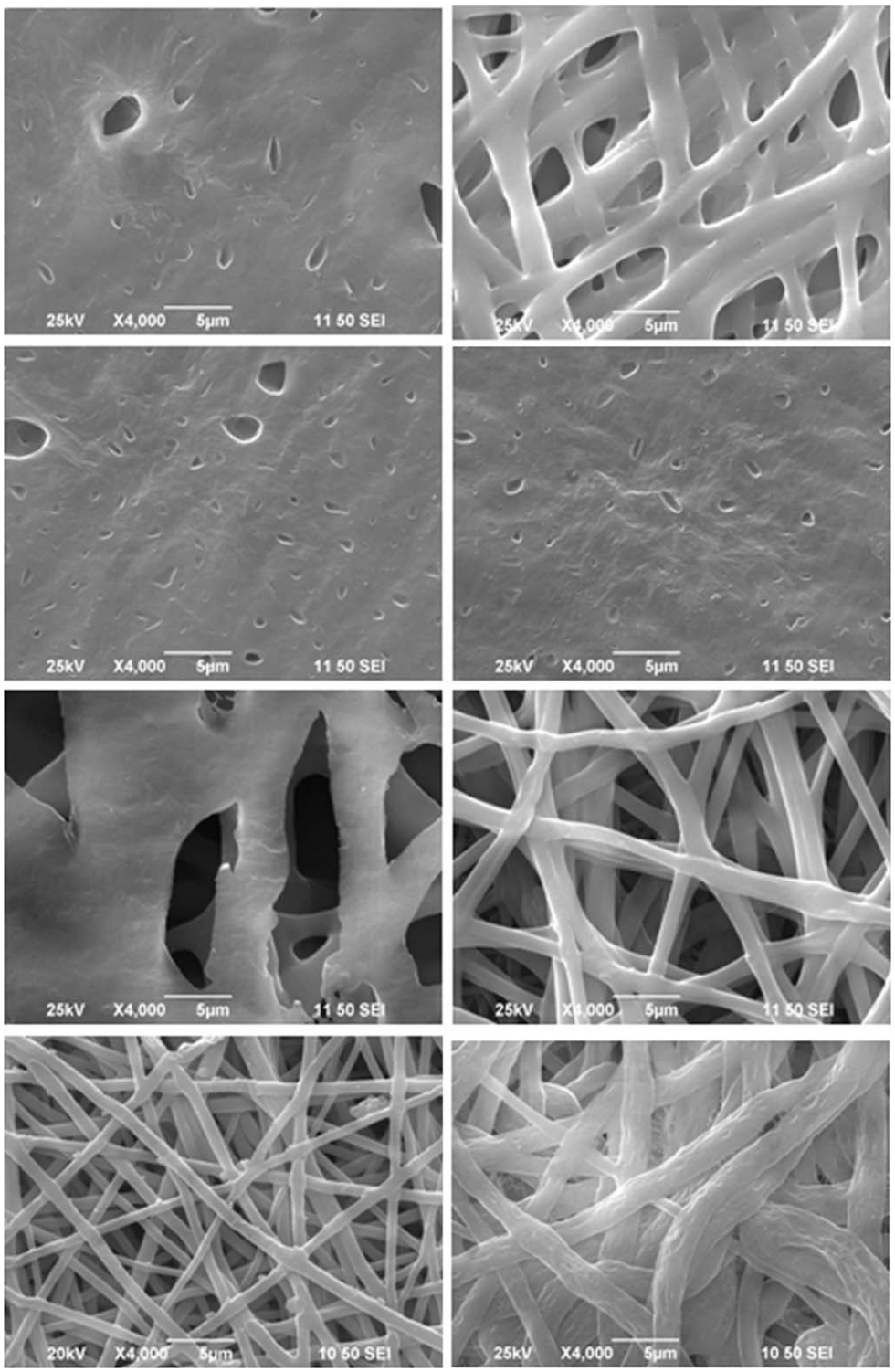


**Figure 5.** SEM micrographs of the PVDF surfaces of the composite membrane.

$$R_m = R_t - R_{up} - R_{in} = R_t - R_{up} - \frac{L_a}{D'_{va}}. \quad (4)$$

where $D'_{va}$ is the equivalent diffusivity of moisture in the air gap and $L_a$ is the air-gap thickness. The two-dimensional effect of moisture in the air-gap exerted an important impact on the results. Therefore, the equivalent diffusivity is proposed here.

The moisture diffusivity of the membrane ($D'_{vf}$) could be calculated with the following equation:

$$D'_{vf} = \frac{\delta}{R_m}^m. \quad (5)$$

where $\delta$ is the thickness of the TFC membrane.

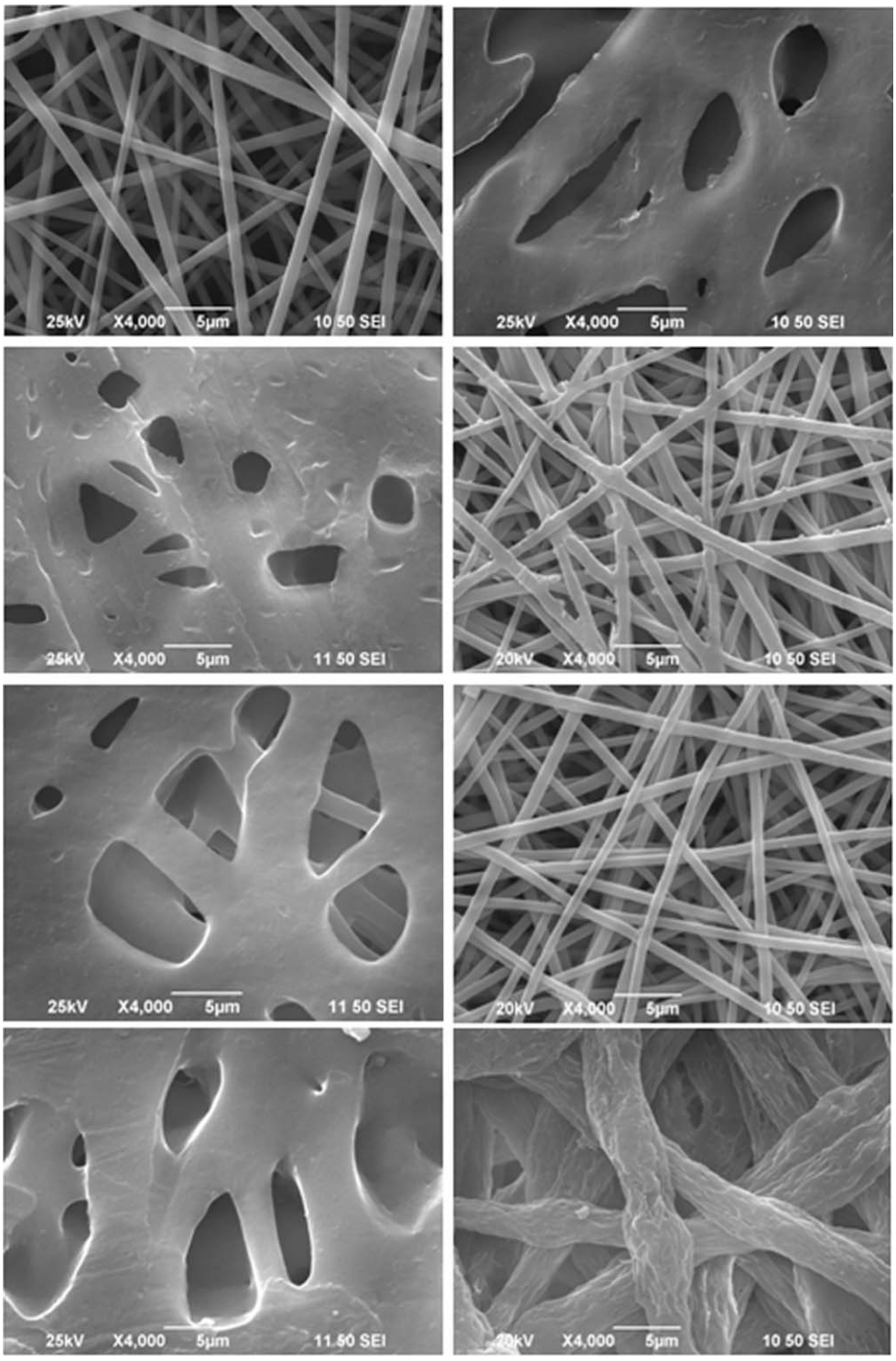


**Figure 5.** (Continued)

To extract $R_m$ of the sample, three kinds of experiments were schemed and implemented to obtain $R_{up}$, the equivalent diffusivity of moisture, and $R_t$, respectively.[23,24] In the first test, the convective moisture transfer coefficient over the membrane was determined with an uncovered cup, whose water surface was directly exposed to an air current. The second test was to exploit the equivalent moisture diffusion coefficient in the air gap through various $L_a$ values. $D'_{va}$ was estimated from the slope of the plot moisture resistance against $L_a$.[23] The linear relationship is validated in the following section. In the third test, we obtained $R_t$ with the same method described in the second test.

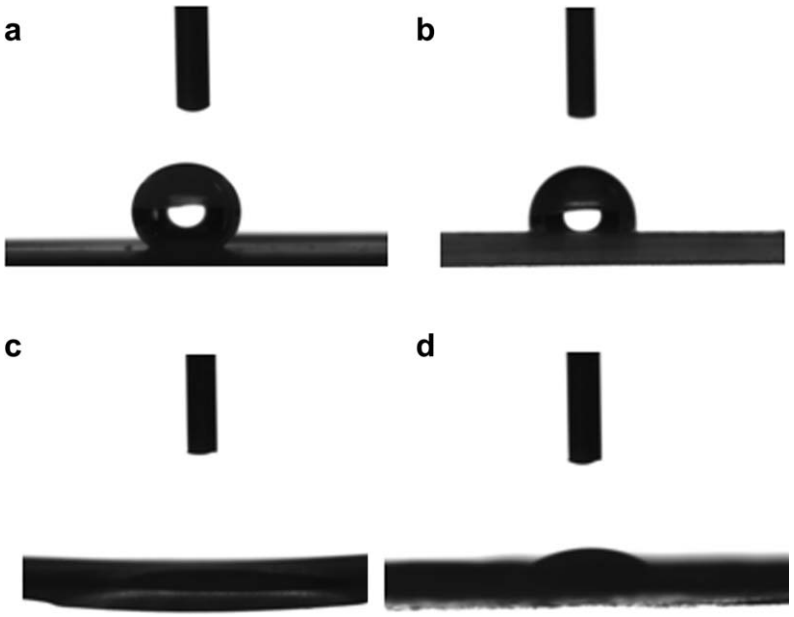


**Figure 6.** Shape of the water droplet on the surface of the membrane: (a) the surface of the PVDF side before hot pressing, (b) the surface of the PVDF side after hot pressing, (c) the surface of the TPEE side before hot pressing, and (d) the surface of the TPEE side after hot pressing.

## RESULTS AND DISCUSSION

### Characterization of the TFC Membrane

The PVDF nanofiber films were prepared by electrospinning from different PVDF aqueous solvent systems according to the orthogonal experimental design method. Figure 5 shows the different morphologies of such PVDF nanofiber mats. The average diameters are also presented in Table II. The morphologies of the electrospun product method were mainly influenced by the concentration of the solution, the solvent, the electric potential, and the nozzle-to-collector distance.[25] No nanofiber shape product was found under the electrospinning condition of low concentration of the solution [Figure 5(a,c,d)]. The solution could produce a stable fluid because of low viscosity. The surface tension of liquid flow was so low that the liquid bead or ball formed in the electrostatic field. Also, a wet and adhering membrane with some sheet microholes was formed after hot-pressing [Figure 5(b,f)]. However, the membrane fabricated at a high concentration presented the characteristics of concave and convex surfaces, small pores, and stack-aligned fibers [Figure 5(h,p)]. These results indicate that the solution concentration was a relatively important parameter in electrospinning in the control of the nanofiber diameter.[26] We observed that the nanofibers in the membrane shown in Figure 5(i) appeared smoothest and most uniform and exhibited the fewest beads and defects. According to Table I (level and factor of orthogonal design), 16 groups of experiments were conducted, and the experimental results of the orthogonal design are shown in Table II. As shown in the table, the nanofiber diameter obtained from the $L_{16}$ orthogonal array experiments ranged from 0 to 4917 nm. The optimum configuration was $A_3B_1C_3D_4C_2$, as determined by the finest fiber diameter. Under such experimental conditions, the finest fiber diameter of the PVDF nanofibrous membrane was 1250 nm. Therefore, we selected the 15% PDVF concentration, 6-kV applied electric field, a ratio of 70% DMAc to 30% acetone, 0.5 g/mL of ACM, and a distance of 14 cm between the spinneret and the collecting drum as the electrospinning parameters for producing the membrane used in the following characterizations.

The wettability used to characterize the surface hydrophilicity or hydrophobicity of the TFC film was estimated by CA analysis with the captive bubble method. The CA images of the PVDF side of the TFC film before heat-pressing and after heat-pressing were 130 and 100°, respectively, as presented in Figure 6(a,b). In general, the wettability of the membrane surface was governed by both the chemical composition and the geometrical microstructure of the surface.[27] The high CA of 130° for the PVDF membrane was an indication of the relatively good hydrophobicity because of the nanostructures and the presence of —CF2— hydrophobic groups. This was because the nanostructure was introduced into the very large fraction of air in the membrane surface, and this prevented water droplets from spreading over the membrane.

The CA images of the TPEE membrane are also shown in the figure. Figure 6(c) displays the shape of the water droplet on the surface of the raw TPEE membrane with a CA of 0°. This reveals the typical hydrophilic characteristics of the TPEE membrane. The polymer material was composed of a large amount of polyester and polyether with a linear molecular chain structure. A higher hydrophilic monomer content certainly resulted in a molecular/ether bond ladder for moisture transmission with much less time.

The surface roughness became smaller when the PVDF or TPEE side was heat-pressed. The surface roughness is a very important factor in wetting.[28] According to the Wenzel equation,[29] the hydrophobicity became more excellent for the hydrophobic

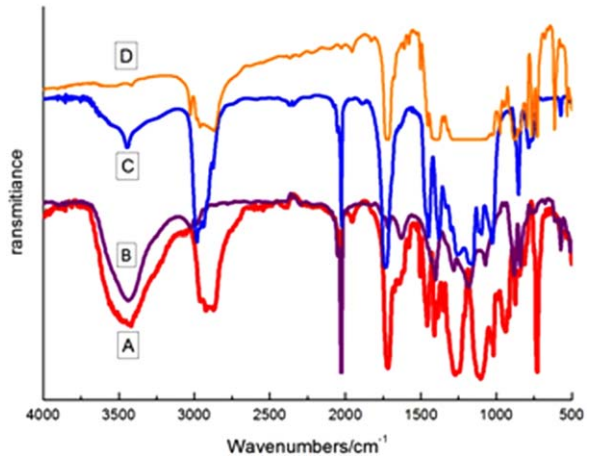


**Figure 7.** ATR–FTIR spectrum of (A) TPEE, (B) PVDF, (C) ACM, and (D) composite membranes. [Color figure can be viewed in the online issue, which is available at wileyonlinelibrary.com.]

membrane with increasing surface roughness. On the contrary, the hydrophilic membrane provided more intense hydrophilicity with increasing surface roughness. Because of the higher roughness, the CA of the PVDF nanofiber membrane before heat pressing was 130°, whereas the CA of the PVDF side after heat pressing was only 100°. The reduction in hydrophilic groups in the TPEE membrane led to a decline in the water-absorbing capacity of the TPEE membrane. The TFC membrane exhibited bipolar characteristics of hydrophilicity and hydrophobicity. This was also the foundation of waterproofness and moisture permeability for the TFC membrane.

The ATR–FTIR spectra of the fingerprint region of TPEE (curve A), PVDF (curve C), ACM, and composite membrane system (curve B) are shown in Figure 7. The IR spectrum of the TFC samples consisted of bands attributed to the TPEE substrate film, PVDF fiber mat, and ACM polymer. Moreover, the distinct peak at 2100 $cm^{-1}$ disappeared, and the new peaks at 735 and 623 $cm^{-1}$ appeared in the TFC membrane spectrum. We deduced that the crosslinking interaction occurred between the TPEE film and ACM polymer, and some new functional groups formed.

Peaks in both the TPEE and composite membrane at 2941 $cm^{-1}$ (—$CH_2$— asymmetric stretching) and 1716 $cm^{-1}$ (C═O stretching), respectively, were characteristic of TPEE.[20] The relatively wide spectra appearing between 1000 and 1450 $cm^{-1}$ were attributed to the overlying results from the peaks at 1447 $cm^{-1}$ (COO— absorption), 1269 $cm^{-1}$ (—O— absorption), and 1072 $cm^{-1}$ (—CF2— absorption) of acrylic acid.

Figure 8 shows the tensile stress and strain curves for the TPEE substrate membrane and TPEE–PVDF composite membrane. The longitudinal and transverse directions were defined by the orientation of the TPEE substrate membrane with winding direction in parallel and perpendicularity, respectively. The composite membrane was also in the case. As shown in the figure, the TFC membrane possessed a stronger tensile stress (longitudinal stress = 5.66 MPa, transverse stress = 4.5 MPa) than that of the TPEE substrate membrane, whose tensile stresses were 4.0 MPa in the longitudinal direction and 3.85 MPa in the transverse direction. A lower elongation at break ratio (longitudinal = 20% and transverse = 60%) occurred in the TFC membrane than in the TPEE substrate membrane (longitudinal = 120% and transverse = 173%). In general, the elongation at break of the membrane increased similarly in the same mode as the tensile stress. However, the absolutely different results of the elongation at break of the sample indicated that the porous structure of the electrospinning nanofiber mat executed an important influence on the elongation at break. The numerous pores forming a looser structure changed the molecular orientation of the nanofiber. Therefore, the elongation at break decreased because of the decrease in the molecular orientation.

### Evaluation of the WVT Performance

Figure 9 shows the regression curves obtained by linear fitting through the experimental data (air layer thickness vs moisture resistance) for the moisture resistance of the TPEE single-layer film and TFC membrane (PVDF/TPEE). The regression equations were shown to be valid because the relative coefficients were larger than 0.91. The test results show that $R_t$ increased almost linearly with $L_a$; this supported the fact that the equivalent diffusivity in the air gap could be estimated from the slope

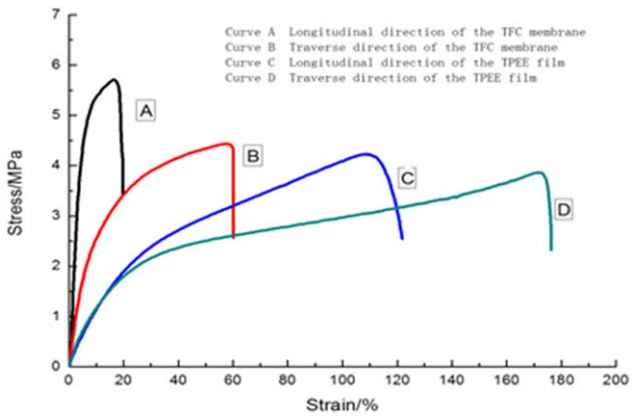


**Figure 8.** Stress–strain curves for the TPEE substrate film and TFC membrane. [Color figure can be viewed in the online issue, which is available at wileyonlinelibrary.com.]

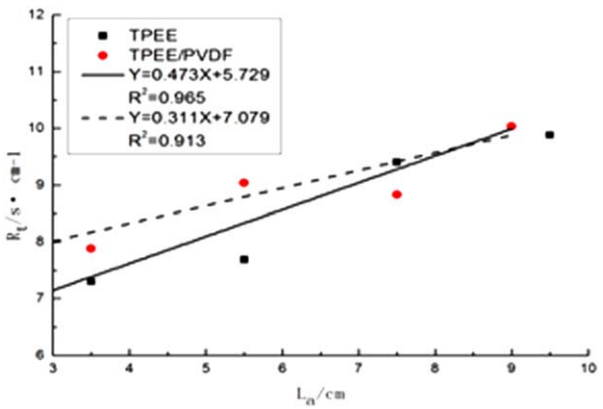


**Figure 9.** Relationship between the moisture resistance and the thickness of the air gap. [Color figure can be viewed in the online issue, which is available at wileyonlinelibrary.com.]

**Table III.** Moisture Resistances and Diffusivities During Testing

| Sample | $R_t$ | $R_{in}$ | $R_m$ | $R_{up}$ | $D'_{va}$ | $D'_{vf}$ |
|---|---|---|---|---|---|---|
| TPEE | 7.299 | 1.656 | 4.095 | 1.548 | $2.114 \times 10^{-5}$ | $3.663 \times 10^{-2}$ |
| PVDF/TPEE | 9.042 | 1.009 | 6.485 | 1.548 | $3.215 \times 10^{-5}$ | — |

of a plot of moisture resistance against $L_a$. $R_t$ and $R_{up}$ above the membrane were obtained according to eq. (2). As shown in eq. (4), $R_m$ of the tested membrane was obtained by the subtraction of the convective resistance and the air-gap resistance from the total resistance. Table III summarizes the values of three moisture resistances for TPEE membrane and PVDF/TPEE composite film.

To characterize the behavior of moisture transfer through the TFC membrane, a resistance-in-series model was proposed on the basis of Henis and Tripodi's resistance model approach.[30] The TFC membrane was prepared by deposition of the PVDF nanofibers onto a nonporous TPEE membrane. The multilayered structure of the TFC membrane is shown in Figure 10(a) and is divided into three fields: the TPEE dense layer, the embedded layer, and the PVDF porous layer. The embedded layer was defined as the region in which the dense layer materials penetrated into the pores of the porous layer.

The moisture transfer through the TFC membrane was analogous to the relationship between the resistances in an electrical circuit. Three different resistances, $R_{up}$, $R_m$, and $R_{in}$ related to the transport could be distinguished.

$R_m$ of the TFC membrane was composed of the four resistances to moisture transport flow and can be described as follows [Figure 10(a,b)]:

1. The resistance of the dense TPEE layer ($R_1$).
2. The resistance of the section where the pores were filled with the TPEE materials within the embedded layer ($R_2$).
3. The resistance of the remaining section where the pores were not filled the TPEE materials within the embedded layer ($R_3$).
4. The resistance of the porous PVDF layer ($R_4$).

It should be noted that $R_2$ was in parallel with $R_3$. According to Henis and Tripodi's electrical circuit analog,[30,31] $R_m$ of the TFC membrane could be written as follows:

$$R_m = R_1 + \frac{R_2 R_3}{R_2 + R_3} + R_4. \quad (6)$$

In the diffusion process, the water vapor concentration gradient ($\Delta c$) acted as a driving force in the transmission of moisture from one side of the TFC membrane to the other. Therefore, the relation between the diffusion flux and $\Delta c$ could be postulated by Fick's law:

$$Q = D\frac{\Delta c}{L}. \quad (7)$$

where $D$ is the diffusion coefficient of the membrane material, $A$ is the membrane surface area, $L$ is the membrane thickness, and $Q$ is the water vapor flux.

$R_m$ was inverse proportion to the term of $D/L$ and could be described as follows:

$$R_m = \frac{\Delta c}{Q} = \frac{L}{DA}. \quad (8)$$

According to eq. (8), each resistance could be rewritten as follows

$$R_1 = \frac{L_1}{D_1 A},\ R_2 = \frac{L_2}{D_1 \cdot A \cdot (1-\zeta)},\ R_3 = \frac{L_2}{D_1 \cdot A \cdot \zeta},\ R_4 = \frac{L_3}{D_2 A}. \quad (9)$$

where $\zeta$ is the surface porosity of the TPEE dense membrane, and this is related to the surface roughness of the material.

Next, we determined the diffusivities of the hydrophilic, dense TPEE material ($D_1$) and the microporous PVDF material ($D_2$) by referring to the published literature on the single-layer membrane.

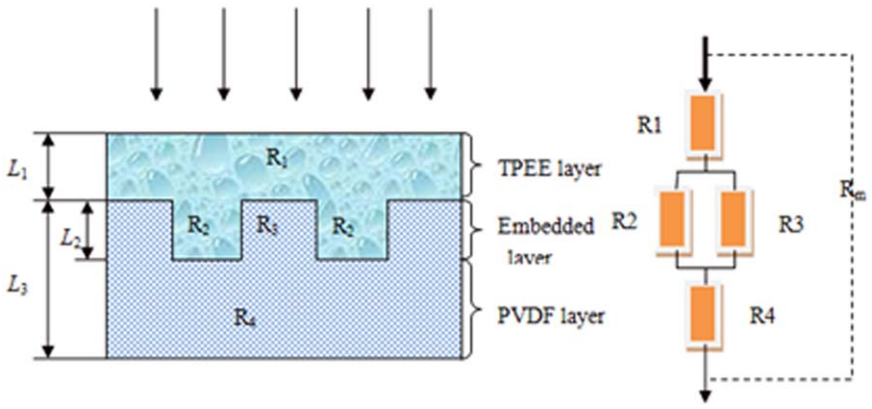


**Figure 10.** Schematic representation of the TFC membrane and the corresponding electrical circuit analog. Schematic diagram of the three-tier composite membrane electrical circuit analog. $L_1$ = thickness of dense TPEE layer; $L_2$ = thickness of the embedded layer; $L_3$ = thickness of the porous PVDF layer. [Color figure can be viewed in the online issue, which is available at wileyonlinelibrary.com.]

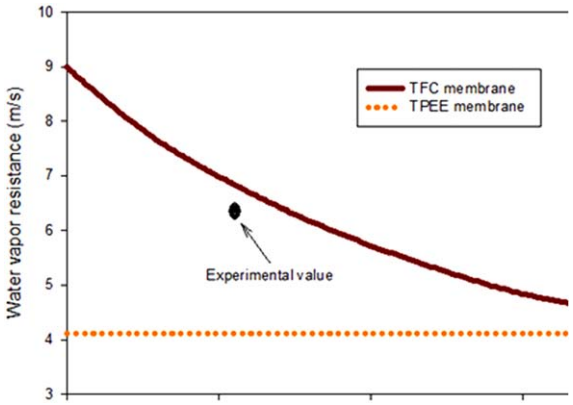


**Figure 11.** Effect of the porosity of the electrospinning PVDF web on the water resistance of the TFC membrane. [Color figure can be viewed in the online issue, which is available at wileyonlinelibrary.com.]

Moisture transport through the dense TPEE membrane was related to the hydrophilic group and could be described by the solution–diffusion model. The water vapor first was adsorbed in the surface of the membrane with a high concentration and then diffused through the membrane because of the driving force the concentration difference. Finally, the water vapor desorbed from the side of the membrane with a low concentration. Finally, the water vapor desorbed from the side of the membrane with a low concentration. An assumption in the use of the diffusion flux definition through the membrane is that the WVT rate through the membrane satisfies Fick's law. Therefore, the water vapor diffusivity of the TPEE membrane could be acquired as follows:[32]

$$D_1 = \frac{e^{5294/T}}{10^6 \rho_a} \times \frac{L_1}{\Delta\phi}. \quad (10)$$

where $T$ is the temperature of the TPEE membrane, $\rho_a$ is the air density and $\Delta\phi$ is the relative humidity difference between two sides of the TPEE membrane. We assumed that the value of relative humidity below the TPEE membrane was 100% RH.

The electrospinning PVDF porous layer had a similar structure to that of fibrous material, whose pore size distribution and pore length were found to be fractal and self-similar, so the fractal geometry theory was applied to develop an analytical model to predict the moisture diffusivity of the PVDF electrospinning membrane. In this study, for simplicity, we considered that only a bundle of cylindrical capillary tubes of differing diameter but equal length existed in the fibrous material [Figure 10(a)].

For the electrospinning PVDF nanofiber membrane (porous layer within the TFC film), the membrane pore sizes were assumed to satisfy the standard normal distribution, that is[33]

$$f(r) = \frac{1}{\sqrt{2\pi}\bar{r}\sigma} \exp\left[-\frac{(1-r/\bar{r})^2}{2\sigma^2}\right]. \quad (11)$$

where $f(r)$ is the probability density function, $\bar{r}$ is the mean pore radius, and $\sigma$ is the dimensionless standard deviation, of which $\bar{r}$ and $\sigma$ determine the pore size distribution.

The transmembrane moisture flux could be calculated over the entire range of pore sizes from minimum ($r_{min}$) to maximum ($r_{max}$). The diffusion in the porous membrane, which varied with resistance to diffusion molecule movement, was mainly controlled by three mechanisms: bulk diffusion ($D_B$), Knudsen diffusion ($D_K$), and surface diffusion. In general, the effect of the surface diffusion can be ignored for no striking absorption in the porous media. In this study, only $D_K$ and $D_B$ were considered in the calculation of the moisture diffusivity. Detailed derivation for $D_B$ and $D_K$ are explained in refs. 34 and 35. $D_2$ for the PVDF porous membrane were calculated with the following equation:[36]

$$D_2 = \frac{\varepsilon P_0}{\rho_a \tau} \frac{\int_0^{r_{max}} f(r)[(D_K^{-1} + D_B^{-1})^{-1}] r^2 dr}{\int_0^{r_{max}} f(r) r^2 dr} \frac{M_a}{M_v} \quad (12)$$

where $L_2$ is the thickness of the PVDF membrane, $\tau$ is the tortuosity of the pore, $\varepsilon$ is the porosity of the PVDF membrane, $r$ is the pore radius, $P_0$ is the water vapor pressure, and $M_v$ and $M_a$ are the molar masses of water vapor and air, respectively.

$R_t$ of the TFC membrane obtained from the calculating model was 6.691 s/cm; this was very close to the experimental value of 6.485 s/cm (Table III). The fact that predicted and measured values were in good agreement confirmed the validity of the basic considerations upon which our model depend.

Figure 11 illustrates that the water vapor resistance within the PVDF/TPEE composite membrane decreased with increasing porosity of the electrospinning PVDF web. When the porosity increased, the water vapor resistance decreased, and the penetrability increased. The change in the TFC membrane moisture permeation performance with the electrospinning fibrous web porosity was obviously the result of the increase in straight channels. Water vapor molecules got across the porous membrane with less resistance.

## CONCLUSIONS

TFC membranes as barrier materials for chemical protective clothing applications were fabricated and characterized in this study. The preparation of the TFC membranes was accomplished by the electrospinning of PVDF nanofibers on a TPEE dense supporting layer; this was followed by a hot-pressing posttreatment. The TFC membrane possessed good mechanical properties, including a greater tensile stress (longitudinal = 5.66 MPa and transverse = 4.5 MPa) than that of the TPEE substrate membrane, whose tensile stress was 4.0 MPa in the longitudinal direction and 3.85 MPa in the transverse direction. The optimized PVDF/TPEE composite membranes fabricated by the single-step method overcame the drawback of incompatibility of the coating solution and the substrate material. WVT rate tests showed that the addition of an electrospinning nanoporous layer onto the TPEE barrier layer did not remarkably weaken the water vapor permeation ability. The results obtained from the proposed moisture resistance in-series model based on Henis–Tripodi's method for the TFC membrane confirmed this conclusion. The TFC membrane water vapor permeation performance could be

simulated very well with the resistance model, and the influence of the porosity of electrospinning PVDF layer on the water vapor permeability of the TFC membrane could also be analyzed.

## ACKNOWLEDGMENTS

We gratefully acknowledge the financial support from the joint project from the Henan–Provincial and the China–National Natural Science Foundations (project number U1304513) and the Key Laboratory of Fire Fighting and Rescuing Technology Foundation of the Ministry of Public Security of China (contract grant number KF201301). The authors declare no competing financial interest.

## REFERENCES

1. Huang, L. W.; McCutcheon, J. R. *J. Membr. Sci.* **2014**, *457*, 162.
2. Huang, S. H.; Jiang, G. J.; Liaw, D. J.; Li, C. L.; Hu, C. C.; Lee, K. R.; Lai, J. Y. *J. Appl. Polym. Sci.* **2009**, *114*, 1511.
3. Zhou, W. Y.; Bahi, A.; Li, Y. J.; Yang, H. J.; Ko, F. *RSC Adv.* **2013**, *3*, 11614.
4. Yoo, K.; Kin, K.; Wang, X. F.; Fang, D. F.; Hsiao, B.; Chu, B. *Polymer* **2006**, *47*, 2434.
5. Hao, X. M.; Zhang, J. C.; Guo, Y. H. *Eur. Polym. J.* **2004**, *40*, 673.
6. Huang, J. Z.; Zhang, J. C.; Gao, W. D. *J. Donghua Univ. (English Ed.)* **2006**, *23*(1).
7. Hao, X. M.; Zhang, J. C.; Guo, Y. H. *J. Donghua Univ. (English Ed.)* **2004**, *21*, 58.
8. Yu, C. H.; Kusumawardhana, I.; Lai, J. H.; Liu, Y. L. *J. Colloid Interface Sci.* **2009**, *336*, 260.
9. Jiang, X.; Ding, J. F.; Kumar, A. *J. Membr. Sci.* **2008**, *323*, 371.
10. Zhou, W. Y.; Bahi, A.; Li, Y. J.; Yang, H.; Ko, F. *RSC Adv.* **2013**, *3*, 11614.
11. Gibson, P.; Gibson, H. S.; Rivin, D. *Colloids Surf. A* **2001**, 187, *469*.
12. Gugliuzza, A.; Drioli, E. *J. Membr. Sci.* **2013**, *446*, 350.
13. Hu, X. L.; Zhou, G. Y.; Huang, Y. B.; Xie, Z. G.; Jing, X. B. *J. Controlled Release* **2014**, *185*, 12.
14. Tijing, L. D.; Choi, W.; Jiang, Z.; Amarjargal, A.; Park, C. H.; Pant, H. R.; Im, I. T.; Kim, C. S. *Curr. Appl. Phys.* **2013**, *13*, 1247.
15. Gopal, R.; Kaur, S.; Feng, C. Y.; Chan, C.; Ramakrishna, S.; Tabe, S.; Matsuura, T. *J. Membr. Sci.* **2007**, *289*, 210.
16. Bui, N. N.; Lind, M. L.; Hoek, E. M. V.; McCutcheon, J. R. *J. Membr. Sci.* **2011**, 385, *10*.
17. Zhang, H. Y.; Zheng, J. F.; Zhao, Z. G.; Han, C. C. *J. Membr. Sci.* **2013**, *442*, 124.
18. Zhao, Z. Z.; Li, J. Q.; Ruean, X. Y.; Li, X.; Zhang, Y. Y.; Sheng, J. *J. Appl. Polym. Sci.* **2005**, *97*, 466.
19. Choi, S. S.; Lee, Y. S.; Joo, C. W.; Lee, S. G.; Park, J. K.; Han, K. S. *Electrochim. Acta* **2004**, *50*, 339.
20. Schledjewski, R.; Schultze, D.; Imbach, K. P. *J. Ind. Text.* **1997**, *27*, 105.
21. Antony, J. *Sens. Rev.* **2006**, *26*, 227.
22. ASTM E96/E96M-14, Standard Test Methods for Water Vapor Transmission of Materials; ASTM International: West Conshohocken, PA, 2014.
23. Woo, S. S.; Shalev, I.; Barker, R. L. *Text. Res. J.* **1994**, *64*, 190.
24. Min, J. C.; Hu, T.; Song, Y. Z. *J. Membr. Sci.* **2011**, *367*, 174.
25. Liao, Y.; Wang, R.; Tian, M.; Qiu, C. Q.; Fane, A. G. *J. Membr. Sci.* **2013**, 425, *30*.
26. Veleirinho, B.; Rei, M. F.; Lopes-Da-Silva, J. A. *J. Polymer Sci.* **2008**, *46*, 460.
27. Feng, L.; Li, S. H.; Li, Y. S.; Li, H. J.; Zhang, L. J.; Zhai, J.; Song, Y. L.; Liu, B. Q.; Jiang, L.; Zhu, D. B. *Adv. Mater.* **2002**, *14*, 1857.
28. Jiang, L.; Zhao, Y.; Zhai, J. *Angew. Chem.* **2004**, *116*, 4438.
29. Wenzel, R. N. *J. Phys. Chem.* **1949**, *53*, 1466.
30. Henis, J. M. S.; Tripodi, M. K. *J. Membr. Sci.* **1981**, *8*, 233.
31. Peng, F. B.; Liu, J. Q.; Li, J. T. *J. Membr. Sci.* **2003**, *222*, 225.
32. Zhu, F. L.; Zhou, Y.; He, J. X. *Therm. Sci.* **2013**, *17*, 1293.
33. Kreyszig, E. Advanced Engineering Mathematics, 7th ed.; Wiley: New York, **1993**.
34. Mason, E. A.; Malinauskas, A. P. Gas Transport in Porous Media: The Dusty-Gas Model; Elsevier: New York, **1983**.
35. Welty, J. R.; Wicks, C. E.; Wilson, R. E. Fundamentals of Momentum, Heat, and Mass Transfer, 3rd ed.; Wiley: New York, **1984**.
36. Min, J. C.; Hu, T. *J. Membr. Sci.* **2011**, *379*, 496.